diode imaged in the plasma on the $CO_2$ laser focal spot shows a twofold increase in light emission (dominantly free-bound and free-free radiation) from that region at the time of the interaction.

The interaction observed in the interferograms appears to be interpretable with classical models. However, the formation of Fresnel rings is only observed when the plasma is initially overdense or slightly underdense. Currently, we are unable to explain this. Furthermore, the Fresnel pattern would indicate a quiescent state; thus, the increased modulation of the transmitted light is also unexpected. Experiments are presently underway to study the power dependence of these phenomena and to time resolve the backscatter. A subnanosecond high-power $CO_2$ laser is under construction so that our experiments will more nearly simulate current laser-pellet experiments.

(The formation of a hard aperture as evidenced by the Fresnel rings, and the propagation of radiation through the initially overdense plasma, have recently been predicted theoretically by Sodha and Tripathi.[18])

The authors gratefully acknowledge the theoretical assistance provided by Dr. James J. Duderstadt, Dr. Donald Kenney, and Dr. Rudi S. Ong. Also, we would like to acknowledge helpful conversations with Dr. Joseph M. Kindel from Los Alamos Scientific Laboratory. This work was supported in part by the National Science Foundation, the Air Force Office of Scientific Research, and the University of Michigan College of Engineering.

[a]Permanent address: Los Alamos Scientific Laboratory, Los Alamos, N. Mex. 87545.

[b]Permanent address: Laboratory for Laser Energetics, College of Engineering and Applied Science, University of Rochester, Rochester, N. Y. 14627.

[1]Damon V. Giovanielli, Bull. Am. Phys. Soc. 21, 1047 (1976).

[2]K. G. Estabrook, E. J. Valeo, and W. L. Kruer, Phys. Fluids 18, 1151 (1975).

[3]D. W. Forslund, J. M. Kindel, Kenneth Lee, and E. L. Lindman, Phys. Rev. Lett. 36, 35 (1976).

[4]H. G. Ahlstrom *et al.*, UCRL Report No. UCRL-77943, 1976 (unpublished).

[5]D. T. Atwood, D. W. Sweeney, J. M. Auerbach, and P. H. Y. Lee, Bull. Am. Phys. Soc. 22, 1060 (1977).

[6]N. J. Peacock *et al.*, Bull. Am. Phys. Soc. 21, 1039 (1976).

[7]D. G. Steel *et al.*, "An Ultradense Reproducible *Z* Pinch Suitable for $CO_2$ Laser-Pellet Simulation Experiments" (to be published).

[8]D. P. Duston, P. D. Rockett, D. G. Steel, J. G. Ackenhusen, D. R. Bach, and J. J. Duderstadt, Appl. Phys. Lett. 31, 801 (1977).

[9]M. A. Uman, *Introduction to Plasma Physics* (McGraw-Hill, New York, 1964).

[10]Spawr Optical Research, Inc., 1521 Pomona Rd., Corona, Calif. 91720.

[11]R. W. MacPherson, Rev. Sci. Instrum. 45, 316 (1974).

[12]M. E. Hufford and H. T. Davis, Phys. Rev. 33, 589 (1929).

[13]O. P. Judd, LASL Report No. LA-5391-MS, 1973 (unpublished).

[14]J. F. Drake *et al.*, Phys. Fluids 17, 778 (1974).

[15]D. W. Forslund, J. M. Kindel, and E. L. Lindman, Phys. Fluids 18, 1002 (1975).

[16]P. D. Rockett, "Extraction of Axial Electron Density Profiles from Abel Invertible Interferograms" (unpublished).

[17]K. A. Brueckner and S. Jorna, Rev. Mod. Phys. 46, 325 (1974).

[18]M. S. Sodha and V. K. Tripathi, Phys. Rev. A 16, 2101 (1977).

## Double-Layer Forward Shocks in a Magnetohydrodynamic Fluid

T. Tajima, J. N. Leboeuf, and J. M. Dawson

*Department of Physics, University of California, Los Angeles, California 90024*

(Received 19 December 1977)

We have observed forward-facing slow wave shocks created by an obstacle in a magnetohydrodynamic flow in runs on a magnetohydrodynamic particle stimulation code. The shocks have a double-layer structure composed of the compressive and accompanying rarefactive slow-wave fronts.

One of the most striking features of the magnetohydrodynamic (MHD) shocks is the possibility of a *forward*-facing (upstream) shock.[1,2] Craig and Paul[3] first observed in a laboratory experiment slow-wave shocks in a one-dimensional configuration. Chao and Olbert[4] inferred the existence of forward slow-wave shocks from solar wind data which showed discontinuities in physi-

cal quantities consistent with the relations predicted by theory. However, experimental[1] or observational[4] difficulties have hampered observing clear evidence of the forward propagation of the shocks so far. We report in the Letter what we believe to be the first direct observation of forward propagation of the slow-wave shocks in runs on a newly developed MHD particle simulation code.[5] The forward slow-wave shocks are created by an obstacle in an MHD flow. We have also observed a novel double-layer structure to the upstream shocks composed of a compressive slow-wave shock and a rarefactive slow-wave front.

Propagation of the phase fronts (characteristics) of shock waves may be most easily depicted by the Friedrichs diagram.[1,2] In contrast to hydrodynamic supersonic shock[6] or MHD fast-wave shock,[1] the Friedrichs diagram for the slow-wave shock has a concave envelope and indicates the possibility of the forward-facing characteristics [see Fig. 1(a)] created by an obstacle. When the Alfvén velocity $V_A$ is larger than the sound velocity $C_s$, for production of slow-wave shocks by the obstacle $v < C_S$ is necessary. The diagram also suggests that there appear skew shock fronts when the magnetic field is tilted with respect to the zeroth-order flow. On the other hand, fast-wave shocks point downstream.

In order to realize the necessary conditions for the shocks and observe them, we set up the MHD code as follows. A plasma is modeled as an ideal dissipationless MHD fluid with isothermal temperature. The equation of motion is integrated in a Lagrangian way employing finite-size particles[7] to represent elements of the fluid. The hydrodynamic pressure force is calculated from the density by utilizing the nearest grid method for finite-size particles and the fast-Fourier-transform technique to find a pressure field, while the Maxwell stress forces are obtained through a finite-differencing scheme to advance the magnetic field. The code is conservative of the magnetic flux, total plasma mass, as well as momentum.[5] We have used a $2\frac{1}{2}$-dimensional (two spatial dimensions and three velocity and field dimensions) version of the code. The most appealing property of the code for the present problem, however, may be the stability of the code: Not only does the code never experience negative-density difficulties, but it also turns out to be stable against local violation of the Courant-Friedrichs-Lewy condition that conventional Eulerian code has to satisfy. Thanks to this property, we are able to investigate the problem of an obstacle in an MHD flow in spite of the formation of the shadow behind the obstacle where the density of particles is very low or even locally zero; there is some sacrifice in accuracy here but not in stability.[5] To stimulate the obstacle, we introduce a force potential $f_0 = \vec{f} \times \exp\{-[(x-x_0)^2 + (y-y_0)^2]/2a^2\}$ which repels the fluid. Initially the particles assume a uniform flow velocity $\vec{v} = \hat{v}x$. A periodic boundary condition is taken for the fields, while the particles crossing through the boundaries at $x = 0$ and $L_x$ are scrambled in their $y$ coordinates after their reentry in order to avoid artificial interference from downstream disturbances affecting the upstream region and vice versa. (There is some effect of this kind due to periodic boundary conditions on the fields but it appears much less important.)

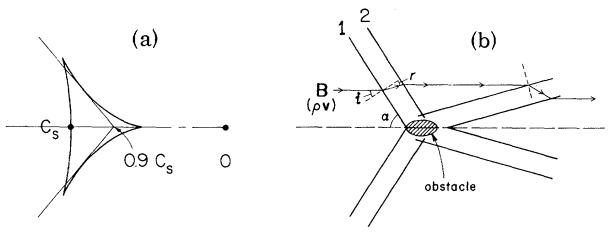


FIG. 1. (a) The Friedrichs diagram and the slow-wave characteristics for $V_A/C_s = 1.5$. (b) Schematic "rays" of $\vec{B}$ and $\rho\vec{v}$ around the obstacle.

Basically two types of runs are performed. The first type is the case where the flow velocity is parallel or antiparallel to the external magnetic field. The second is one where the flow velocity is oblique to the magnetic field. Under an appropriate choice of parameters one expects for the first case symmetric forward shocks with respect to $y = y_0$. For the second case, tilted shock fronts should appear as predicted by the Friedrichs diagram [Fig. 1(a)]. We have chosen $2 \times 2$ particles in a cell, the system size $L_x \times L_y = 32\Delta \times 32\Delta$ with $\Delta$ being the cell length, the particle half-width $= 1\Delta$, $\vec{f}/m_i = 0.8C_s^2$, $a = 1.0\Delta$, and $x_0 = y_0 = 16\Delta$. When we increase the number of particles in a cell and/or the system size we have not observed any significant qualitative difference from the present choice. Figure 2 shows the results of the simulation of the parallel type of flow at $t = 30C_s/\Delta$. The Mach number $M = v/C_s = 0.9$ and $V_A/C_s = (\beta/2)^{1/2} = M/A = 1.5$ ($A$ being the Alfvén number) have been taken. In each frame of Fig. 2 are seen discontinuity fronts at the

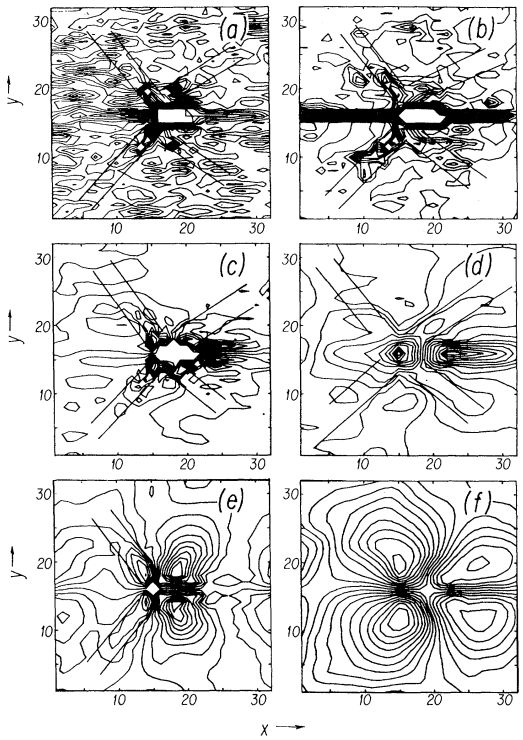


FIG. 2. Contour plots of the flow and field quantities with $\vec{B} \parallel \vec{v}$. The flow is from left to right and the obstacle is located at the center of the diagrams. Each has twenty contours. (a) Density contour; the lowest contour (LC) is 0, the highest (HC) 12.4. (b) Velocity in $x$ contour; LC $= -0.218$, HC $= 1.024$. (c) Velocity in $y$ contour; LC $= -0.221$, HC $= 0.212$. (d) $B_x$ contour; LC $= -0.102$, HC $= 0.087$. (e) $B_y$ contour; LC $= -0.055$, HC $= 0.057$. (f) The magnetic field lines excluding the external field.

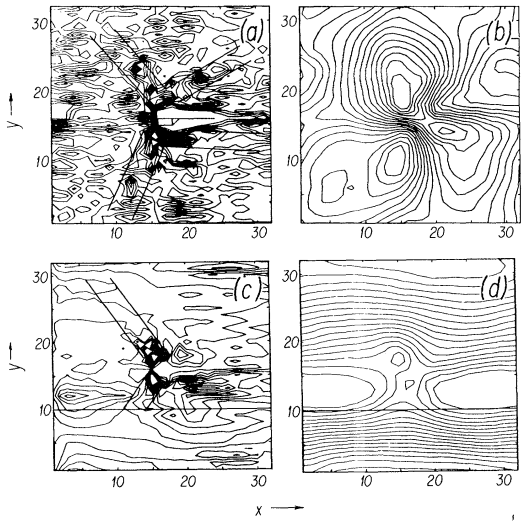


FIG. 3. Contour plots of the flow and field quantities with oblique magnetic field. The flow is still from left to right. Each has twenty contours. The last two frames are $\vec{B} \parallel \vec{v}$ but with temperature gap. (a) Density contour; LC $= 0$, HC $= 11.4$. (b) $B_x$ contour; LC $= -0.122$, HC $= 0.069$. (c) $V_y$ contours. (d) The magnetic field lines for the case $C_s' = 1\sqrt{3}\,C_s$ and $\rho' = 3\rho$ where the primed quantities are in $y = [0, 10]$. $\vec{B} \parallel \vec{v}$ and $V_A/C_s$ 1.5.

same positions stretching forward from the obstacle with the same shock angle $\alpha = 52°$ with respect to the magnetic field. The angle $\alpha$ predicted by the diagram is 49.6°. After an initial transient period, this structure emerges and becomes clear about $t = (15\text{–}20)C_s/\Delta$; afterwards it maintains a rather stationary pattern with a slow stretching of its fronts until $t = 35C_s/\Delta$. Later the pattern becomes chaotic due to reentering field interference. Figures 3(a) and 3(b) exhibit the oblique case at $t = 30C_s/\Delta$ with $M = 0.9$, $V_A/C_s = 1.505$, and $B_{y0}/B_{x0} = 0.09$. The forward-stretching fronts tilt at approximately the same angles as predicted by theory [Fig. 1(a)]. In addition we, as expected, do not observe any forward-facing fronts, for example, in the case of $M = 2.0$, $V_A/C_s = 1.5$. These signatures along with the following analysis of the jump conditions strongly suggest that forward-facing slow-wave shocks have been observed in these model calculations.

In the fine structure of the patterns in Fig. 2 one notices a double-layer structure composed of two parallel forward-stretching fronts as schematically exemplified in Fig. 1(b). The width of the double layer is constant in time and approximately $2\Delta$. As one closely examines the jump conditions of physical quantities across each discontinuity line, one can conclude that the leading front, 1, in fact satisfies all the conditions associated with the compressive slow-wave shock, while the latter front, 2, satisfies jump conditions for the rarefactive slow wave. The set of ideal MHD equations for a steady isothermal flow embraces[8,9] a class of solutions of the type

$$\vec{B} = \epsilon\rho\vec{v}, \tag{1}$$

where $\rho$ is the mass density and $\epsilon$ is assumed here a constant determined by the boundary conditions at infinity. If the flow is parallel to the external magnetic field, $\epsilon > 0$, and if antiparallel, $\epsilon < 0$. Introducing the unit normal $\vec{n}$ to the spatial discontinuity and transverse unit vector $\vec{t}$ orthogonal to $\vec{n}$, and writing $\vec{v} - v_n\vec{n} \equiv \vec{v}_t = v_t\vec{t}$ and $v_n = \vec{v}\cdot\vec{n}$, the characteristic equations[9] for $\rho$, $v_n$,

and $v_t$ are

$$\delta v_n = -v_n \delta\rho/\rho, \tag{2}$$

$$\rho v_n \delta v_n + \rho \vec{v}_t \cdot \delta \vec{v}_t + C_s^2 \delta\rho = 0, \tag{3}$$

$$(\epsilon^2/4\pi)\delta(\rho \vec{v}_t) = \delta \vec{v}_t, \tag{4}$$

where $\delta$ denotes the jump of each quantity from the downstream to the upstream. $\nabla \cdot \vec{B} = 0$ implies $\delta B_n = 0$ and

$$\delta \vec{B}_t = (4\pi/\epsilon)\delta \vec{v}_t. \tag{5}$$

Equations (2) through (5) reduce to

$$(v_n^2 - C_s^2)\delta\rho/\rho = \vec{v}_t \cdot \delta \vec{v}_t, \tag{6}$$

$$(v_n^2 - C_s^2)/v^2 = (M^2 - 1)/A^2 M^2. \tag{7}$$

Equation (7) gives the theoretical value of the shock angle as $\alpha = \sin^{-1}[(M^2 + A^2 - 1)/A^2 M^2]^{1/2} = 49.7°$, which is again in good agreement with the simulation. For a compressive change $\delta\rho > 0$ and for a rarefactive change $\delta\rho < 0$; for a slow-wave shock $M < 1$ and for a fast-wave shock $M > 1$. From Eqs. (6) and (7)

$$\delta v_t > 0 \text{ when } [\delta\rho < 0,\ M < 1] \text{ or } [\delta\rho > 0,\ M > 1], \tag{8}$$

$$\delta v_t < 0 \text{ when } [\delta\rho > 0,\ M < 1] \text{ or } [\delta\rho < 0,\ M > 1]. \tag{9}$$

With the aid of Eq. (5), the above implies that if $\epsilon > 0$ and $M - 1 < 0$

$$\delta B_t < 0 \text{ for } \delta\rho > 0, \tag{10}$$

$$\delta B_t > 0 \text{ for } \delta\rho < 0. \tag{11}$$

Either of the sign changes in $\epsilon$ and $M - 1$ will reverse the inequalities in Eqs. (10) and (11). From the simulation results [Fig. 2(a)] we learn that $\delta\rho > 0$ at the discontinuity 1 and $\delta\rho < 0$ at 2. From Figs. 2(d) and 2(e) we find that $\delta B_t < 0$ at 1 and $\delta B_t > 0$ at 2; from Figs. 2(b) and 2(c) we obtain $\delta v_t < 0$ at 1 and $\delta v_t > 0$ at 2. We also note that when we ran the cases with $\vec{B}$ antiparallel to $\vec{v}$ ($\epsilon < 0$), we had $\delta v_t < 0$ and $\delta B_t > 0$ at 1 and $\delta v_t > 0$ and $\delta B_t < 0$ at 2, as is suggested by the relation given by Eq. (5). Therefore, from simulation we find the magnetic pressure difference $\delta P_M < 0$ at 1 and $\delta P_M > 0$ at 2 for both $\epsilon > 0$ and $\epsilon < 0$. All these findings are consistent with Eqs. (8)–(11).

Moreover, once $\delta\rho$ is known, other theoretical jump conditions may be calculated through Eqs. (2)–(5) and can be compared to the simulation results. We find $\delta\rho^1 = 1.96 \pm 0.4$ and $\delta\rho^2 = 1.95 \pm 0.4$, where the superscript refers to the discontinuity, either 1 or 2. Consequently, the simulational and theoretical values are $\delta v_n{}^1 = (0.26 \pm \pm 0.06)C_s$ [$-0.39$], $\delta v_n{}^2 = (0.21 \pm 0.16)C_s$ [0.24]; $\delta v_t{}^1 = (0.042 \pm 0.016)C_s$ [0.036], $\delta v_t{}^2 = (0.028 \pm 0.016)C_s$ [0.024]; $|\delta v_{At}{}^1|(\propto B_t{}^1) = (0.021 \pm 0.009)C_s$ [0.018], $|\delta v_{At}{}^2|(\propto B_t{}^2) = (0.017 \pm 0.0008)C_s$ [0.028]; and $\delta P_M{}^1 = -0.064$, $\delta P_M{}^2 = 0.043$. Here the quantities in brackets correspond to the theoretical coefficients. Thus not only the signs of the jumps are in agreement with the theoretical prediction, but also the absolute values are quite consistent with the theory. Possible reasons for the deviations may come from (i) error in the assumption that $\epsilon$ is constant in the theory, (ii) reading of discrete contour lines, and (iii) numerical errors in the simulation.

One may be able to interpret Fig. 1(b) in terms of a "Snell-like" law. Since $\delta B_n = 0$, $\tan r/\tan i = 1 + \delta B_t/B_t$, where $i$ and $r$ are the incident and "refractive" angles of $\vec{B}$ (and $\rho\vec{v}$), and a weak shock is assumed. Utilizing Eqs. (5)–(7) and noting $4\pi/\epsilon^2 = A^2\rho$, we obtain

$$\frac{\tan r}{\tan i} = 1 + \frac{\delta\rho}{\rho}\frac{1}{A^2 - 1}. \tag{12}$$

Across each front the $\vec{B}$ and $\rho\vec{v}$ vectors "refract" more deeply or more shallowly depending on the sign of the density jump. Formation of the double layers may be physically understood. Since the fluid element "sees" the obstacle, it deflects off the obstacle or stagnation point at 1. After it travels past the obstacle it sees the vacuum behind the object and starts to flow into this region and thus the stream line should bend the other way at 2. Eventually it should come back to the original $y$ coordinate, which also creates disturbances downstream as seen in Fig. 2 (= the second double-layer downstream). Since in the upper half-plane ($y > y_0$) $v_y > 0$ in front of the obstacle, $v_y < 0$ behind it, the current induced by $\vec{v} \times \vec{B}$ sets up a current flow pattern (= the upstream double layer and the downstream double layer) which leads to the quadrupole structure in the magnetic field lines illustrated in Fig. 2(f). In contrast to the present subsonic flow, we have observed only a dipole magnetic line structure in the supersonic flow case. This is because the flow past the obstacle in the latter case does not squeeze its stream lines in the shadow area, but it carries field lines away from the obstacle.

Finally we mention the case of runs where the

lower $\frac{1}{3}$ of the fluid ($y \leq 10\Delta$) had $\frac{1}{3}$ the temperature and three times the density of the rest of the fluid; then in the lower area the slow-shock conditions do not apply. The forward shock front seems to be discontinued at around the $y = 10\Delta$ boundary in this case [see Fig. 3(c)]. In addition we no longer observe the quadrupole pattern but instead the pattern in Fig. 3(d).

The authors are grateful for communications with Dr. T. Taniuti, Dr. C. F. Kennel, Dr. F. Coroniti, Dr. S. Hashiguchi, Dr. K. Mima, Dr. A. Hertzberg, and Dr. H. Hasimoto. This work was supported by the National Science Foundation, Grant No. PH4-15233.

[1]W. R. Sears, Rev. Mod. Phys. 32, 701 (1960).
[2]H. Hasimoto, Rev. Mod. Phys. 32, 860 (1960).
[3]A. D. Craig and J. Paul, Phys. Rev. Lett. 30, 681 (1973).
[4]J. K. Chao and S. Olbert, J. Geophys. Res. 75, 6394 (1970).
[5]J. N. Leboeuf, T. Tajima, and J. M. Dawson, to be published.
[6]L. Landau and E. Lifshitz, *Fluid Mechanics* (Pergamon, New York, 1959), p. 310.
[7]C. K. Birdsall, A. B. Langdon, and H. Okuda, *Methods in Computational Physics* (Academic, New York, 1970), Vol. 9, p. 241.
[8]H. Grad, Rev. Mod. Phys. 32, 830 (1960).
[9]A. Jeffrey and T. Taniuti, *Nonlinear Wave Propagation* (Academic, New York, 1964), p. 293.

## Observation of the Orientation Dependence of Interface Dipole Energies in Ge-GaAs

R. W. Grant, J. R. Waldrop, and E. A. Kraut
*Science Center, Rockwell International, Thousand Oaks, California 91360*
(Received 19 December 1977)

The interfaces between a thin (~ 20-Å) abrupt epitaxial layer of Ge grown on substrates of (111), (110), and (100) GaAs have been investigated with x-ray photoelectron spectoscopy. Observed changes in core-level binding energies have been directly related to the crystallographic orientation dependence of interface dipoles and variations of band-gap discontinuities. The orientation variation of the band-gap discontinuities is found to be a significant fraction ($\approx \frac{1}{4}$) of the total band-gap discontinuity.

There has been considerable theoretical interest in the properties of ideal abrupt interfaces between different semiconductors, stimulated in part by the recent progress in molecular beam epitaxy (MBE) whereby truly abrupt interfaces can now be achieved. A basic property of the abrupt semiconductor interface is the relative alignment of the energy bands of the two semiconductors; i.e., how the energy difference in the band gaps ($\Delta E_g$) is distributed between the valence- and conduction-band discontinuities ($\Delta E_v$ and $\Delta E_c$) such that $\Delta E_g = \Delta E_v + \Delta E_c$.

The first and most widely used model for estimating $\Delta E_c$ (or $\Delta E_v$) is based on electron affinity differences.[1] Critical evaluations[2,3] have been made of this model. Alternative models for predicting $\Delta E_v$ have appeared,[4,5] and two self-consistent calculations of the Ge/GaAs-interface electronic structure have been completed.[6,7] Although it has long been recognized that interface dipoles could produce energy-band discontinuities which depend on crystallographic orientation of the interface plane, such effects have generally been ignored. Transport measurements[8] on vapor-grown Ge/GaAs heterojunctions suggested that there could be substantial (a few tenths of an eV) changes in valence- and conduction-band discontinuities, $\delta(\Delta E_v)$ and $\delta(\Delta E_c)$, dependent on crystallographic orientation. Unfortunately, it is relatively difficult to determine these dopant-level-independent quantities from transport measurements and the scatter in these data is as large as the measured effect.

To investigate the interface dipole orientation dependence, we have developed a contactless x-ray photoemission spectroscopy (XPS) technique which allows a direct probe of interface potential variations. Herein, we report the observation of sizable and systematic variations in $\Delta E_v$ for the Ge/GaAs interface as a function of crystallographic orientation. Figure 1 is a schematic energy-band diagram of an ideal abrupt Ge/GaAs interface. The relative positions of the average bulk crystal potential within the two semiconductors determine $\Delta E_v$ and $\Delta E_c$.[2,4-6] An orientationally dependent change in the interface dipole magnitude may shift the relative positions of the valence and conduction bands in the two semiconductors as shown schematically by dashed lines in Fig. 1. Figure 1 also shows the position of a

 